Rapid Communications

Continuous doping of a cuprate surface: Insights from *in situ* angle-resolved photoemission

Y.-G. Zhong,[1,2] J.-Y. Guan,[1,2] X. Shi,[1,2,*] J. Zhao,[1,2] Z.-C. Rao,[1,2] C.-Y. Tang,[1,2] H.-J. Liu,[1,2] Z. Y. Weng,[3,4] Z. Q. Wang,[5] G. D. Gu,[6] T. Qian,[1,4] Y.-J. Sun,[1,7,8,†] and H. Ding[1,2,4,7,†]

[1]*Beijing National Laboratory for Condensed Matter Physics and Institute of Physics, Chinese Academy of Sciences, Beijing 100190, China*
[2]*School of Physics, University of Chinese Academy of Sciences, Beijing 100190, China*
[3]*Institute for Advanced Study, Tsinghua University, Beijing 100084, China*
[4]*Collaborative Innovation Center of Quantum Matter, Beijing 100190, China*
[5]*Department of Physics, Boston College, Chestnut Hill, Massachusetts 02467, USA*
[6]*Condensed Matter Physics and Materials Science Department, Brookhaven National Laboratory, Upton, New York 11973, USA*
[7]*CAS Center for Excellence in Topological Quantum Computation, University of Chinese Academy of Sciences, Beijing 100190, China*
[8]*Songshan Lake Materials Laboratory, Dongguan, Guangdong 523808, China*

(Received 29 June 2018; published 24 October 2018)

We report a technique of a continuously doped surface of $Bi_2Sr_2CaCu_2O_{8+x}$ through ozone/vacuum annealing and a systematic measurement over the nearly whole superconducting dome on the same sample surface by *in situ* angle-resolved photoemission spectroscopy. We find that the quasiparticle weight on the antinode is proportional to the doped carrier concentration x within the entire superconducting dome, while the nodal quasiparticle weight changes more mildly. More significantly, we discover that a d-wave pairing energy gap extracted from the nodal region scales well with the onset temperature of the Nernst signal. These findings suggest that the emergence of superconducting pairing is concomitant with the onset of free vortices.

DOI: 10.1103/PhysRevB.98.140507

High-T_c cuprate superconductors distinguish themselves from conventional BCS superconductors in that a small variation in the carrier doping can significantly change the superconducting transition temperature (T_c), giving rise to a superconducting dome and a similarly dome-shape Nernst temperature (T_v) for the onset of superconducting vortices well above T_c [1–3]. In the so-called underdoped (UD) region, a pseudogap [4,5] with highly controversial origins emerges at a temperature much higher than T_c and T_v, whereas the system appears to gradually approach a Fermi liquid in the overdoped (OD) region. Therefore, a systematic study of the properties [6–8] over the whole superconducting dome is critical for understanding the cuprate superconducting mechanism. However, in many families of cuprates, such as $Bi_2Sr_2CaCu_2O_{8+x}$ (Bi2212), high-quality crystals can be only obtained within a narrow doping range. Moreover, surface cleaving, necessary for surface techniques such as angle-resolved photoemission spectroscopy (ARPES) and scanning tunneling spectroscopy (STS) which have studied Bi2212 extensively [2,9], possesses a serious problem for quantitative comparisons from sample to sample. There have been previous endeavors to *in situ* dope the surface of cuprates by evaporating potassium or gas absorption [10–12], however, these methods introduce disorders to the surface that can affect the measured quantities.

Realizing that the doping level in this material is solely controlled by the excess oxygen concentration, we develop a method of ozone/vacuum annealing to continuously change the doping levels of the surface layers, which are subsequently measured by *in situ* ARPES [Figs. 1(a)–1(c)]. Through this technique, we are able to obtain precise quantities of the energy gaps including the pseudogap and the coherent spectral weight over a wide range of doping, revealing important physical insights for the cuprates. In this Rapid Communication, we demonstrate that the quasiparticle weight is linearly proportional to the doped carrier concentration x at the antinode, while it changes much more slowly with doping at the node. By extracting the gap slope around the node region, we discover that the d-wave component of the quasiparticle energy gap is linearly proportional to the Nernst temperature T_v over the entire superconducting dome, strongly suggesting that the emergence of superconducting pairing is accompanied by the onset of free vortices, with direct implications for the strong fluctuation of the superconducting (SC) phase far beyond T_c.

Optimally doped Bi2212 single crystals were grown by the floating-zone technique. We refer to heating samples in an ultrahigh vacuum and ozone atmosphere as vacuum annealing and ozone annealing, respectively. A high-quality optimally doped single crystal was cleaved in a vacuum better than 1×10^{-7} Torr, then degassed in a molecular beam epitaxy (MBE) chamber to ensure a clean surface, and annealed at $\sim$470 °C in the ozone atmosphere with a partial pressure of about 4×10^{-6} Torr for 15 min to obtain a highly overdoped surface. The doping level of the surface was then reduced by a series of vacuum annealing processes with increasing heating power. After each annealing process, the sample was transferred *in situ* to an ARPES chamber for measurements. The freshness of a sample surface can be regenerated through each annealing process, and a sample surface can be measured over 1 month without noticeable contamination. The *in situ* ARPES measurements were carried in an ARPES system

*Present address: Department of Physics and JILA, University of Colorado and National Institute of Standards and Technology (NIST), Boulder, CO 80309, USA.

†Corresponding authors: yjsun@iphy.ac.cn; dingh@iphy.ac.cn

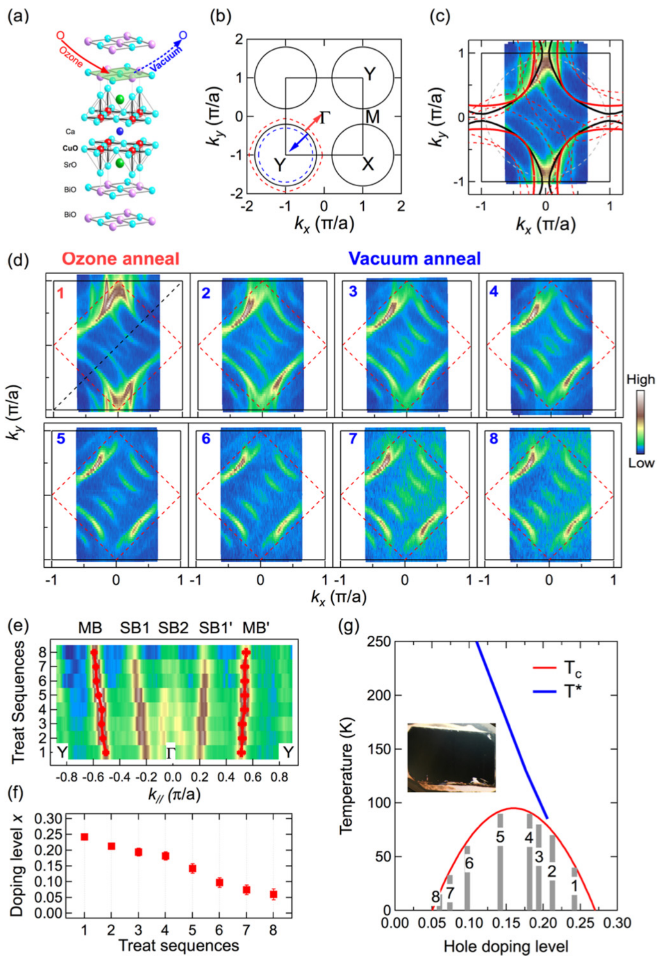

FIG. 1. (a) Crystal structure of Bi2212, and the schematic of ozone annealing (red arrows) and vacuum annealing (blue arrows) surface treatments. (b) The schematic FS of Bi2212 after ozone (red) and vacuum annealing (blue). (c) The FS of the OD one with considerations of superlattice FS (red dashed line) and shadow FS (gray dashed line). The bold black and red lines are the fitting results corresponding to the antibonding and bonding FS, respectively. Those FSs are acquired at 30 K by integrating ±10 meV around E_F. (d) The FS evolution with surface treatment sequences: Ozone annealing (panel 1), and a series of vacuum annealing (panels 2–8). (e) Image plot of the integrated intensity in the vicinity of E_F along the Γ-Y direction for each panel in (d), showing two main bands (MB, MB′), two first superlattice bands (SB1, SB1′), and second superlattice bands (SB2). (f) The extracted doping level of each sequence. (g) The phase diagram of Bi2212: The red line is T_c calculated with an empirical formula [35], the blue line is T^* extracted from the antinodal gap closed temperature, the gray bars are the doping level for each sequence obtained in (f), and the inset picture is the one taken on the cleaved surface of this sample.

equipped with a Scienta R4000 analyzer and a Scienta VUV source. The HeI α resonant line ($h\upsilon = 21.218$ eV) was used, and the vacuum of the ARPES chamber was better than 3×10^{-11} Torr. The energy and angular resolution was set at $\sim$5 meV and 0.2°, respectively.

It is well established that the electronic structure of doped CuO_2 planes of Bi2212 exhibits two-dimensional Fermi-surface (FS) sheets whose area relative to the Brillouin zone area is equal to $(1 + x)/2$, where x is the doped carrier concentration [13]. Therefore, a precise determination of the FS area by high-resolution ARPES, after taking extra care with the superlattice and shadow FSs [Fig. 1(c)] [14], will provide the value of the carrier concentration on the surface. Figures 1(d)–1(g) illustrate an example of how we continuously change the doping level and the corresponding FS contour on one surface. Here, we list a few noticeable features of the FS evolution: (1) There is a continuous reduction of the spectral weight on the FS going from the overdoped (OD) to underdoped (UD) region, especially around the antinodal region, which is mainly caused by the increasing superconducting gap and the emergence of a pseudogap in the UD region. (2) The bilayer splitting [15], clearly visible in the OD region, gradually vanishes in the UD region due to the incoherent c-axis tunneling between adjacent CuO_2 planes. (3) The shrinkage of the FS area can be clearly visualized by the synchronized movement of the main FS and superlattice FSs along the nodal direction [Fig. 1(e)]. A simple fitting to the measured FS [14] yields the carrier concentration of the surface [Fig. 1(f)]. Remarkably, a wide doping range within a nearly full SC dome can be continuously tuned on a single Bi2212 surface [Fig. 1(g)]. Such a "phase-diagram-on-surface" (PDS) method not only extends the doping range beyond the conventional single-crystal method, but also eliminates the uncontrolled influence on the ARPES spectral weight due to the different flatness of the cleaved surfaces, thus enabling a precise analysis and a comparison of important quantities over the phase diagram of the cuprates.

One of the important quantities is the quasiparticle spectral weight (Z), which has been studied extensively by ARPES [16,17]. Despite intensive efforts, reliable quantitative results of the doping evolution of Z and its momentum dependence are difficult to obtain due to its sensitivity to the surface condition that varies from sample to sample. The PDS method overcomes this problem. A coherent quasiparticle peak emerges in the superconducting state [Figs. 2(a) and 2(b)], especially around the antinodal region, whose spectral weight (Z_{AN}) is believed to be related to the superfluid density or the superconducting phase stiffness [18]. Previous ARPES studies [16,17] have indeed revealed that Z_{AN} is proportional to x below the optimal doping level. However, the behavior of Z_{AN} on the overdoped side is controversial, with initial reports of saturating [16] or decreasing [17] behaviors. Figures 2(a) and 2(c) reveal that Z_{AN} on the antinodal FS is linearly proportional to x within the entire superconducting dome. We note that a saturating behavior is observed for the coherent weight at the M point that is not on the FS [14]. In the meantime, the PDS method also enables a precise measurement of the nodal quasiparticle weight (Z_N) that is known to be highly sensitive to the surface flatness. It is clear from Figs. 2(b) and 2(c) that the doping evolution of Z_N is much milder than that of Z_{AN}: It stays almost constant for a wide region on both sides of the optimal doping level, and decreases in the more underdoped region, possibly due to the appearance of a Coulomb gap or other incoherent processes with heavy underdoping [19].

Another important quantity that can be systematically studied by the PDS method is the quasiparticle energy gap in

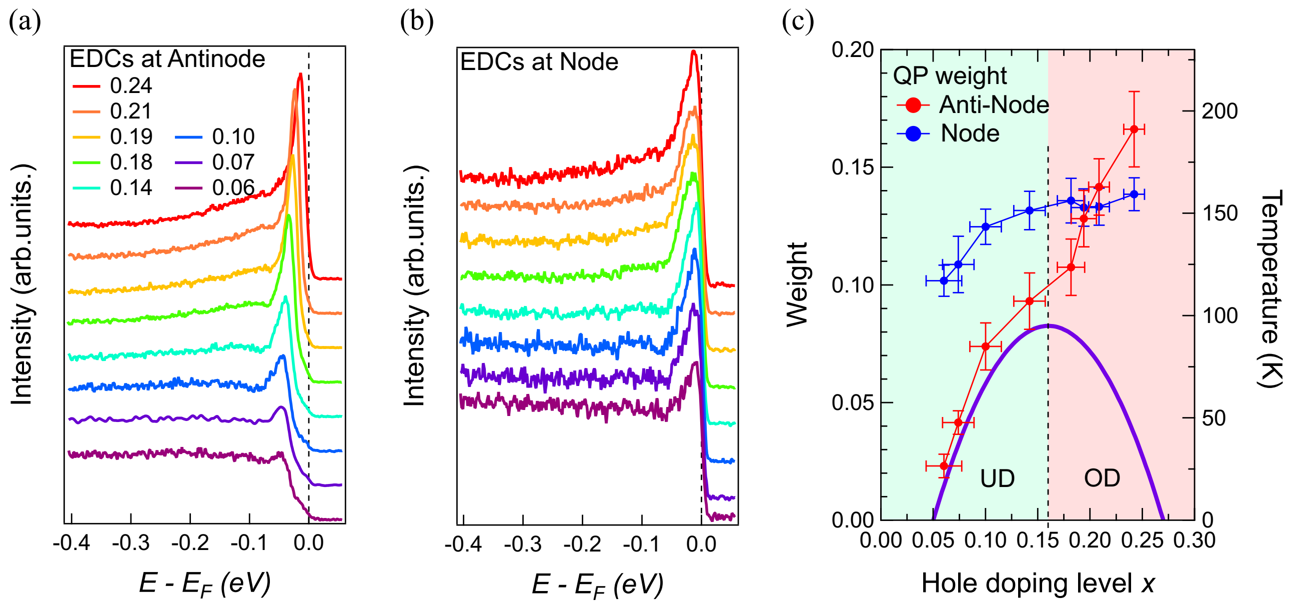

FIG. 2. (a) Antinodal energy distribution curves (EDCs) at k_F evolution with doping. (b) Nodal EDCs at k_F evolution with doping measured on the same sample at 10 K. (c) The extracting quasiparticle weight of the node and the antinode. The T_c line is plotted with the violet color.

the one-electron spectral function, which is a manifestation of both the superconducting gap and the possible pseudogap [4–6]. Since sharp quasiparticle peaks can be observed in the superconducting state at a low temperature, their peak position can be used as a good measure of the energy gap. The symmetrized peaks [20] remove the effect of the Fermi-Dirac function and thus give more precise values of the energy gap along the FS. We summarize the momentum dependence of the energy gap over a wide doping range ($0.07 \leqslant x \leqslant 0.24$) in Figs. 3(a)–3(f). In the OD region, e.g., $x = 0.24$ and 0.21, the momentum dependence of the energy gap follows the $\cos k_x - \cos k_y$ function nicely, reflecting the nature of a single d-wave pairing gap in this region. However, starting from $x = 0.18$, the energy gap extracted from the quasiparticle position deviates upward from the simple d-wave function, and the deviation increases as the doping decreases [21]. This

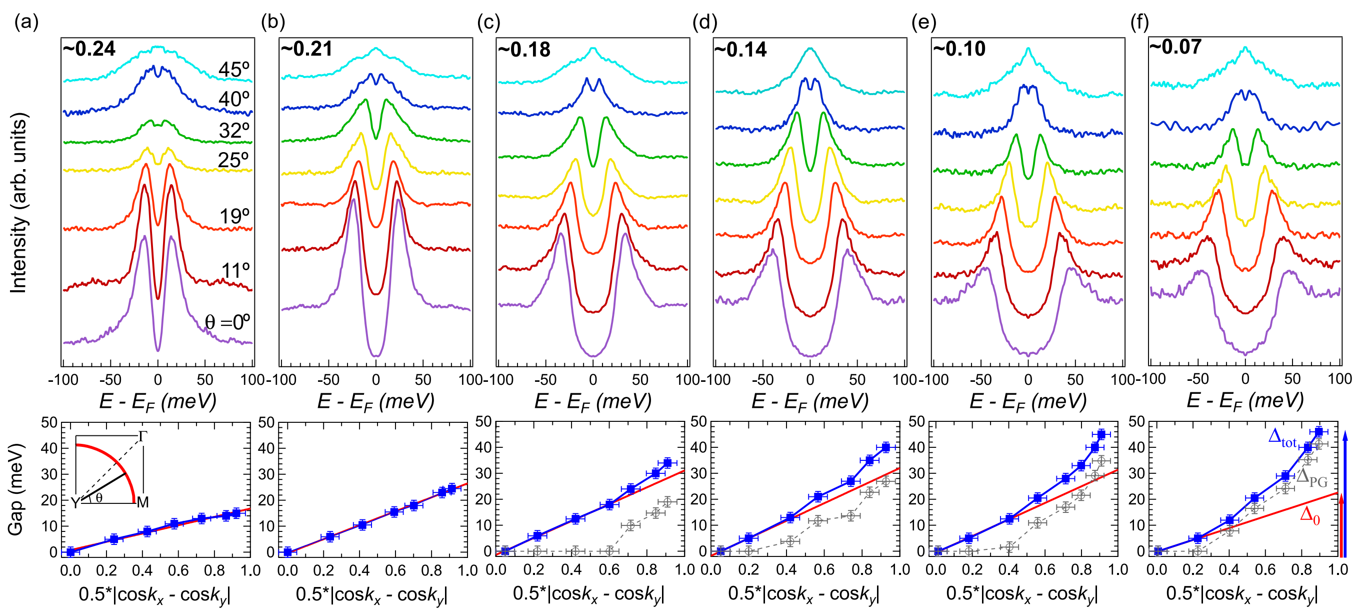

FIG. 3. (a)–(f) The upper panels display the symmetrized EDCs along the FS of six different doping levels. All data are measured on a same sample and a same temperature of ∼10 K. The corresponding momentum positions are indicated in a schematic diagram of FS in the inset of the lower panel of (a). The lower panels display the spectral gap along the FS (plotted against $0.5|\cos k_x - \cos k_y|$) for different doping levels. The blue marked one is the total spectral gap, which is determined from the peak position of symmetrized EDCs, the red line is the corresponding d-wave gap function (for details, see the Supplemental Material [14]) for each doping, and the gray marked one is the pseudogap obtained as describe in the text.

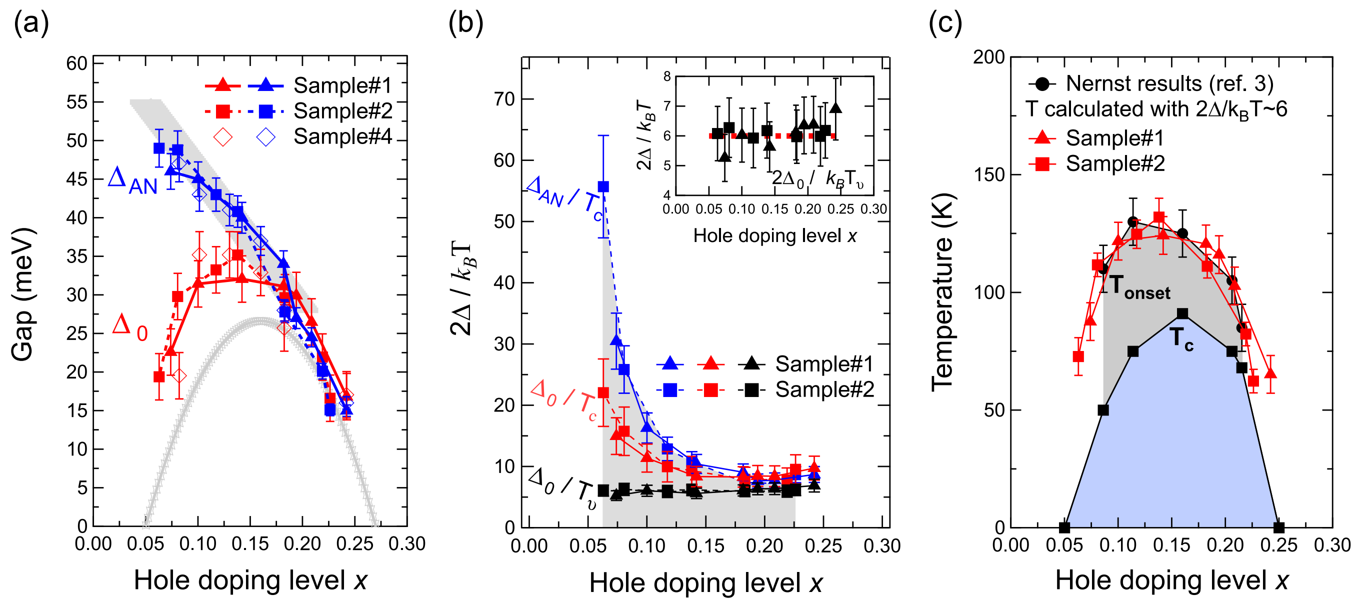

FIG. 4. (a) Doping dependence of the antinode gap Δ_{AN} and *d*-wave gap slope Δ_0. The red symbols are Δ_0, the blue ones Δ_{AN}, and the gray ones the T_c-scaled gap, with three different symbols (solid square, triangle, and spaced rhombus) for three independent samples. (b) Doping dependence of $2\Delta/k_BT_c$. The blue symbols are $2\Delta_{AN}/k_BT_c$, the red ones $2\Delta_0/k_BT_c$, and the black ones $2\Delta_0/k_BT_\upsilon$. The inset is a zoom-in plot to highlight the constant ratio of $2\Delta_0/k_BT_\upsilon$. The Nernst temperatures of the doping levels that are not included in Ref. [3] are estimated from a polynomial fitting to the data in Ref. [3]. (c) A phase diagram of Bi2212. The red symbols are the pairing temperatures obtained from the constant ratio with Δ_0, the black dots the onset temperatures of the Nernst signal from Ref. [3], and the black square ones the superconducting transition temperatures.

is indicative of the opening of the pseudogap whose origin has been widely debated [22,23]. It has been pointed out that the underlying superconducting gap follows the *d*-wave line visibly near the nodal region and extrapolates to the antinodal region, namely, it follows the gap slope (Δ_0) [7,8]. We adopt this method that linearly extrapolates the superconducting gap around the node to the antinode [14] for all the doping levels [lower panels in Figs. 3(a)–3(f)]. If we regard the quasiparticle peak position as the superposition by quadrature of two energy gaps, as suggested previously [24,25], we can then decompose the total spectral gap (Δ_{tot}) into two gaps, $\Delta_{tot} = \sqrt{(\Delta_0^2 + \Delta_{PG}^2)}$, where Δ_0 and Δ_{PG} are the pairing gap and the pseudogap, respectively [Fig. 3(f)]. While the pairing gap, which is extrapolated from the nodal region, follows the *d*-wave function throughout the superconducting dome, the pseudogap opens up first at the antinodal region in the slightly OD region, and spreads toward the nodal region as the doping is reduced. We note that such a decomposition procedure is consistent with the observation of the pseudogap and the Fermi arc phenomena in the normal state above T_c in the UD regime.

Previous ARPES work [8] on single crystals of several doping levels suggested that this extrapolated energy gap is linearly proportional to T_c. However, a more precise study using our PDS method gives a qualitatively different result. Through a careful comparison between the gap at the antinode (Δ_{AN}) and the extrapolated gap (Δ_0), we find that the value of the extrapolated *d*-wave gap Δ_0 locates systematically in between the antinodal gap Δ_{AN} and the energy gap that would scale with T_c [Fig. 4(a)]. In the OD region, these two gaps and the T_c-scaled gap match very well. However, they start to diverge in the UD region, and the coupling strengths $2\Delta/k_BT_c$ obtained using these two gaps increase rapidly in the UD region [Fig. 4(b)], suggesting that neither T^* nor T_c are the thermal correspondence of the nodal *d*-wave gap in the quantum electronic state at low temperatures. Remarkably, if we replace T_c with the Nernst temperature T_υ [3], which was generally identified as a sign of Cooper pair formation, then $2\Delta_0/k_BT_\upsilon$ is nearly a constant over the whole SC dome [Fig. 4(b)], strongly indicating that the extrapolated gap Δ_0 represents a pairing energy gap associated with the formation of Cooper pairs, with a thermal correspondence to T_υ [Fig. 4(c)]. We note that the Nernst signal has been also interpreted as the contribution from the charge carrier (quasiparticle), not necessarily from the superconducting fluctuation [26].

While we showed that the extrapolated nodal *d*-wave gap as the pairing energy scale related to T_υ, the origin of the pseudogap highlighted by the spectral gap around the antinode in the UD region remains an open question. Our measurements alone cannot rule out the scenario that the pseudogap stems from preformed pairs [25,27]. However, the divergent behavior of Δ_{PG} and Δ_0 naturally supports the notion that the pseudogap is due to competing order, such as in the proposed scenarios of charge or bond order [28], valence bond glass [29], pair density wave [30], and loop current [31]. Recent experiments have indeed provided strong evidence for charge order in the UD region [28]. Although we have not observed direct evidence for charge order here, there is a residual spectral weight buildup below the antinodal coherent peak, forming an "antinodal foot" in the UD region [Fig. 2(a) and Fig. S6 in Ref. [14]]. It would be interesting in the future to study whether this antinodal foot is related to the charge order.

Our systematic measurements reveal a two-component coherent peak structure near the Fermi level over a wide range of doping. One has a d-wave-like gap Δ_0 near the nodal region with a much more slowly changing coherent peak weight versus doping. But the characteristic energy Δ_0 itself is shown to scale with the Nernst temperature T_υ, rather than T_c, by a ratio $2\Delta_0/K_BT_\upsilon \sim 6$ over the SC dome [Fig. 4(b)]. Here, T_υ can be interpreted as the onset of the pairing transition before pairing coherence is established, while the Nernst signal comes from the vortices of the local pairing order parameter above T_c. Namely, the difference between T_υ and T_c is due to the destruction of superconductivity by vortex fluctuations instead of vanishing Δ_0, and the true SC phase coherence is established at T_c. The region between T_υ and T_c is anomalously large compared to conventional BCS superconductors, which is possibly a reflection of the energetically favorable vortex core states in the cuprates [1]. Note that the value of the ratio ~6 is comparable to the ratio of $2\Delta_0/K_BT_c$ between 4.6 and 5.6 [32] in the heaviest elemental superconductors such as Hg and Ir, which are in the strong-coupling regime.

In contrast, an antinodal coherent peak with its spectral weight linearly proportional to x is observed to persist beyond the optimal doping. Previously, the antinodal weight has been argued to be related to the superfluid density in the SC state [16–18]. However, the superfluid density has been carefully measured in the overdoped regime of La-214 and found to decrease with a reduction of T_c [33]. Thus, our finding indicates that the antinodal spectral weight scales with the total carrier density x doped into the Mott insulating parent state over the entire superconducting composition. In the underdoped to optimally doped regions, they condense into the superfluid, whereas a significant portion may fail to condense in the overdoped region, in sharp contrast to the BCS theory. It remains to be seen whether theories of doped Mott insulators [1,34] may account for the present ARPES observations.

We thank J.-J. Li, W.-Y. Liu, R.-T. Wang, J.-Q. Lin, F.-Z. Yang, and S.-F. Wu for technique assistance and thank Q. J. Chen, K. Levin, J. X. Li, M. Randeria, and F. C. Zhang for useful discussions. The work at IOP is supported by the grants from the Ministry of Science and Technology of China (2016YFA0401000, 2016YFA0300600, 2015CB921300, 2015CB921000), the Natural Science Foundation of China (11227903, 11574371, 11622435, 11474340), the Chinese Academy of Sciences (XDB07000000, XDPB08-1, QYZDB-SSW-SLH043), and the Beijing Municipal Science and Technology Commission (Z171100002017018). Z.Q.W. is supported by the U.S. Department of Energy (DOE), Basic Energy Sciences Grant No. DE-FG02-99ER45747. G.D.G. is supported by the office of Basic Energy Sciences, Division of Materials Science and Engineering, U.S. DOE, under Contract No. DE-SC0012704.

Y.-G.Z. carried out the ARPES experiments with contributions from X.S., J.Z., Z.-C.R., C.-Y.T., H.-J.L., and T.Q.; J.-Y.G. carried out the ozone annealing; Y.-G.Z. carried out the vacuum annealing; G.D.G. synthesized the single crystals; Y.-G.Z. and H.D. preformed the data analysis, figure development, and wrote the paper with contributions from Z.Y.W., Z.Q.W., Y.-J.S., and J.-Y.G.; Y.-J.S. and H.D. supervised the project. All authors discussed the results and interpretation.

Y.-G.Z. and J.-Y.G. contributed equally to this work.

[1] P. A. Lee, N. Nagaosa, and X.-G. Wen, Doping a Mott insulator: Physics of high-temperature superconductivity, Rev. Mod. Phys. **78**, 17 (2006).

[2] A. Damascelli, Z. Hussain, and Z.-X. Shen, Angle-resolved photoemission studies of the cuprate superconductors, Rev. Mod. Phys. **75**, 473 (2003).

[3] Y. Wang, L. Li, and N. Ong, Nernst effect in high-T_c superconductors, Phys. Rev. B **73**, 024510 (2006).

[4] H. Ding, T. Yokoya, J. Campuzano, T. Takahashi, M. Randeria, M. Norman, T. Mochiku, K. Kadowaki, and J. Giapintzakis, Spectroscopic evidence for a pseudogap in the normal state of underdoped high-T_c superconductors, Nature (London) **382**, 51 (1996).

[5] A. Loeser, Z.-X. Shen, D. Dessau, D. Marshall, C. Park, P. Fournier, and A. Kapitulnik, Excitation gap in the normal state of underdoped $Bi_2Sr_2CaCu_2O_{8+\delta}$, Science **273**, 325 (1996).

[6] M. Hashimoto, I. M. Vishik, R.-H. He, T. P. Devereaux, and Z.-X. Shen, Energy gaps in high-transition-temperature cuprate superconductors, Nat. Phys. **10**, 483 (2014).

[7] I. Vishik, M. Hashimoto, R.-H. He, W.-S. Lee, F. Schmitt, D. Lu, R. Moore, C. Zhang, W. Meevasana, and T. Sasagawa, Phase competition in trisected superconducting dome, Proc. Natl. Acad. Sci. USA **109**, 18332 (2012).

[8] H. Anzai, A. Ino, M. Arita, H. Namatame, M. Taniguchi, M. Ishikado, K. Fujita, S. Ishida, and S. Uchida, Relation between the nodal and antinodal gap and critical temperature in superconducting Bi2212, Nat. Commun. **4**, 1815 (2013).

[9] Ø. Fischer, M. Kugler, I. Maggio-Aprile, C. Berthod, and C. Renner, Scanning tunneling spectroscopy of high-temperature superconductors, Rev. Mod. Phys. **79**, 353 (2007).

[10] M. Hossain, J. Mottershead, D. Fournier, A. Bostwick, J. McChesney, E. Rotenberg, R. Liang, W. Hardy, G. Sawatzky, and I. Elfimov, *In situ* doping control of the surface of high-temperature superconductors, Nat. Phys. **4**, 527 (2008).

[11] Y. Zhang, C. Hu, Y. Hu, L. Zhao, Y. Ding, X. Sun, A. Liang, Y. Zhang, S. He, and D. Liu, *In situ* carrier tuning in high temperature superconductor $Bi_2Sr_2CaCu_2O_{8+\delta}$ by potassium deposition, Sci. Bull. **61**, 1037 (2016).

[12] A. Kaminski, S. Rosenkranz, H. Fretwell, M. Norman, M. Randeria, J. Campuzano, J. Park, Z. Li, and H. Raffy, Change of Fermi-surface topology in $Bi_2Sr_2CaCu_2O_{8+\delta}$ with doping, Phys. Rev. B **73**, 174511 (2006).

[13] H. Ding, M. R. Norman, T. Yokoya, T. Takeuchi, M. Randeria, J. C. Campuzano, T. Takahashi, T. Mochiku, and K. Kadowaki, Evolution of the Fermi Surface with Carrier Concentration in $Bi_2Sr_2CaCu_2O_{8+\delta}$, Phys. Rev. Lett. **78**, 2628 (1997).

[14] See Supplemental Material at http://link.aps.org/supplemental/10.1103/PhysRevB.98.140507 for details of the origins of the superlattice and shadow Fermi surfaces, the fitting procedure

for the Fermi surface, the extracting procedure for the quasiparticle weight and gap slope around the node, and the leading edge foot of the EDCs in the UD region, which includes Refs. [15,16,36–42].

[15] D. L. Feng, N. P. Armitage, D. H. Lu, A. Damascelli, J. P. Hu, P. Bogdanov, A. Lanzara, F. Ronning, K. M. Shen, H. Eisaki, C. Kim, J.-i. Shimoyama, K. Kishio, and Z. X. Shen, Bilayer Splitting in the Electronic Structure of Heavily Overdoped $Bi_2Sr_2CaCu_2O_{8+\delta}$, Phys. Rev. Lett. **86**, 5550 (2001).

[16] H. Ding, J. R. Engelbrecht, Z. Wang, J. C. Campuzano, S.-C. Wang, H.-B. Yang, R. Rogan, T. Takahashi, K. Kadowaki, and D. G. Hinks, Coherent Quasiparticle Weight and its Connection to High-T_C Superconductivity from Angle-Resolved Photoemission, Phys. Rev. Lett. **87**, 227001 (2001).

[17] D. Feng, D. Lu, K. Shen, C. Kim, H. Eisaki, A. Damascelli, R. Yoshizaki, J.-i. Shimoyama, K. Kishio, G. Gu *et al.*, Signature of superfluid density in the single-particle excitation spectrum of $Bi_2Sr_2CaCu_2O_{8+\delta}$, Science **289**, 277 (2000).

[18] P. W. Anderson, The resonating valence bond state in La_2CuO_4 and superconductivity, Science **235**, 1196 (1987).

[19] Z.-H. Pan, P. Richard, Y.-M. Xu, M. Neupane, P. Bishay, A. V. Fedorov, H. Luo, L. Fang, H.-H. Wen, Z. Wang, and H. Ding, Evolution of Fermi surface and normal-state gap in the chemically substituted cuprates $Bi_2Sr_{2+x}Bi_xCuO_{6+\delta}$, Phys. Rev. B **79**, 092507 (2009).

[20] M. Norman, H. Ding, M. Randeria, J. Campuzano, T. Yokoya, T. Takeuchi, T. Takahashi, T. Mochiku, K. Kadowaki, and P. Guptasarma, Destruction of the Fermi surface in underdoped high-T_c superconductors, Nature (London) **392**, 157 (1998).

[21] N. Zaki, H.-B. Yang, J. D. Rameau, P. D. Johnson, H. Claus, and D. G. Hinks, Cuprate phase diagram and the influence of nanoscale inhomogeneities, Phys. Rev. B **96**, 195163 (2017).

[22] T. Timusk and B. Statt, The pseudogap in high-temperature superconductors: An experimental survey, Rep. Prog. Phys. **62**, 61 (1999).

[23] S. Hüfner, M. Hossain, A. Damascelli, and G. Sawatzky, Two gaps make a high-temperature superconductor? Rep. Prog. Phys. **71**, 062501 (2008).

[24] M. Civelli, M. Capone, A. Georges, K. Haule, O. Parcollet, T. D. Stanescu, and G. Kotliar, Nodal-Antinodal Dichotomy and the Two Gaps of a Superconducting Doped Mott Insulator, Phys. Rev. Lett. **100**, 046402 (2008).

[25] C.-C. Chien, Y. He, Q. Chen, and K. Levin, Two-energy-gap preformed-pair scenario for cuprate superconductors: Implications for angle-resolved photoemission spectroscopy, Phys. Rev. B **79**, 214527 (2009).

[26] O. Cyr-Choinière, R. Daou, F. Laliberté, C. Collignon, S. Badoux, D. LeBoeuf, J. Chang *et al.*, Pseudogap temperature T^* of cuprate superconductors from the Nernst effect, Phys. Rev. B **97**, 064502 (2018).

[27] R. Boyack, Q. Chen, A. A. Varlamov, and K. Levin, Cuprate diamagnetism in the presence of a pseudogap: Beyond the standard fluctuation formalism, Phys. Rev. B **97**, 064503 (2018).

[28] R. Comin and A. Damascelli, Resonant x-ray scattering studies of charge order in cuprates, Annu. Rev. Condens. Matter Phys. **7**, 369 (2016).

[29] K.-Y. Yang, T. M. Rice, and F.-C. Zhang, Phenomenological theory of the pseudogap state, Phys. Rev. B **73**, 174501 (2006).

[30] A. Melikyan and Z. Tešanović, Model of phase fluctuations in a lattice d-wave superconductor: Application to the Cooper-pair charge-density wave in underdoped cuprates, Phys. Rev. B **71**, 214511 (2005).

[31] C. Varma, Non-Fermi-liquid states and pairing instability of a general model of copper oxide metals, Phys. Rev. B **55**, 14554 (1997).

[32] B. Mitrović, H. Zarate, and J. Carbotte, The ratio $2\Delta_0/k_BT_c$ within Eliashberg theory, Phys. Rev. B **29**, 184 (1984).

[33] I. Božović, X. He, J. Wu, and A. Bollinger, Dependence of the critical temperature in overdoped copper oxides on superfluid density, Nature (London) **536**, 309 (2016).

[34] Z.-Y. Weng, Mott physics, sign structure, ground state wave function, and high-T_c superconductivity, Front. Phys. **6**, 370 (2011).

[35] M. Presland, J. Tallon, R. Buckley, R. Liu, and N. Flower, General trends in oxygen stoichiometry effects on T_c in Bi and Tl superconductors, Phys. C **176**, 95 (1991).

[36] H. Ding, A. F. Bellman, J. C. Campuzano, M. Randeria, M. R. Norman, T. Yokoya, T. Takahashi, H. Katayama-Yoshida, T. Mochiku, K. Kadowaki, G. Jennings, and G. P. Brivio, Electronic Excitations in $Bi_2Sr_2CaCu_2O_8$: Fermi Surface, Dispersion, and Absence of Bilayer Splitting, Phys. Rev. Lett. **76**, 1533 (1996).

[37] P. Aebi, J. Osterwalder, P. Schwaller, H. Berger, C. Beeli, and L. Schlapbach, Complete Fermi surface mapping of Bi-cuprates, J. Phys. Chem. Solids **56**, 1845 (1995).

[38] N. L. Saini, J. Avila, A. Bianconi, A. Lanzara, M. C. Asensio, S. Tajima, G. D. Gu, and N. Koshizuka, Topology of the Pseudogap and Shadow Bands in $Bi_2Sr_2CaCu_2O_{8+\delta}$ at Optimum Doping, Phys. Rev. Lett. **79**, 3467 (1997).

[39] P. Aebi, J. Osterwalder, P. Schwaller, L. Schlapbach, M. Shimoda, T. Mochiku, and K. Kadowaki, Complete Fermi Surface Mapping of $Bi_2Sr_2CaCu_2O_{8+x}$ (001): Coexistence of Short Range Antiferromagnetic Correlations and Metallicity in the Same Phase, Phys. Rev. Lett. **72**, 2757 (1994).

[40] R. S. Markiewicz, S. Sahrakorpi, M. Lindroos, Hsin Lin, and A. Bansil, One-band tight-binding model parametrization of the high-T_c cuprates including the effect of k_z dispersion, Phys. Rev. B **72**, 054519 (2005).

[41] A. Kaminski, J. Mesot, H. Fretwell, J. C. Campuzano, M. R. Norman, M. Randeria, H. Ding, T. Sato, T. Takahashi, T. Mochiku, K. Kadowaki, and H. Hoechst, Quasiparticles in the Superconducting State of $Bi_2Sr_2CaCu_2O_{8+\delta}$, Phys. Rev. Lett. **84**, 1788 (2000).

[42] J. Mesot, M. R. Norman, H. Ding, M. Randeria, J. C. Campuzano, A. Paramekanti, H. M. Fretwell, A. Kaminski, T. Takeuchi, T. Yokoya, T. Sato, T. Takahashi, T. Mochiku, and K. Kadowaki, Superconducting Gap Anisotropy and Quasiparticle Interactions: A Doping Dependent Photoemission Study, Phys. Rev. Lett. **83**, 840 (1999).